Residual Stresses in 21-6-9 Stainless Steel Warm Forgings

Wesley A Everhart[1], Jordan D Lee[1], Daniel J Broecker[2], John P Bartow[1], Jamie M McQueen[1], Nathan T Switzner[1], Tod M Neidt[1], Thomas A Sisneros[3], and Donald W Brown[3]
[1]Materials Engineering, Honeywell Federal Manufacturing & Technologies, LLC Kansas City, MO, U.S.A. operated for the United States Department of Energy under Contract Number DE-NA0000622.
[2]Materials Science & Engineering, Missouri University of Science and Technology, Rolla, MO, U.S.A.
[3]Lujan Center, Los Alamos Neutron Science Center, Los Alamos, NM, U.S.A.

ABSTRACT

Forging residual stresses are detrimental to the production and performance of derived machined parts due to machining distortions, corrosion drivers and fatigue crack drivers. Residual strains in a 21-6-9 stainless steel warm High Energy Rate Forging (HERF) were measured via neutron diffraction. The finite element analysis (FEA) method was used to predict the residual stresses that occur during forging and water quenching. The experimentally measured residual strains were used to calibrate simulations of the three-dimensional residual stress state of the forging. ABAQUS simulation tools predicted residual strains that tend to match with experimental results when varying yield strength is considered.

INTRODUCTION

Forging

Metals are formed into a desired shape by forging. Forging processes are desirable to attain refinement of the microstructure, increase in strength, and beneficial directionality of properties. Warm forging is deformation of the work piece at a low enough temperature to avoid dynamic recrystallization and grain [1]. Forgings are typically machined into a final shape for tight dimensional tolerances, better surface finish, and lighter weight for end product use. Rather than annealing or heat treating, austenitic stainless steel forgings are often machined in the as-forged state to take advantage of their increased strength, improved microstructure, and realigned segregation after warm forging [2]. Because of the potential for sensitization, many stainless steel forgings are rapidly cooled by water quenching.

Generation of Residual Stresses

The varying cooling rate and temperature gradient during water quenching generates non-uniform plastic flow and development of residual stresses [3]. Water quenching is one of many ways to generate residual stresses. Withers and Bhadeshia [4] identified three categories for the origins of residual stresses: chemical additions, plastic deformation, and thermal treatments. Nitriding would be an example of a chemical addition causing compressive residual stress on the work piece surface. Similarly, shot peening or the forging process itself would exemplify plastic deformation for surface compressive residual stresses. Water quenching would fall

within the thermal treatment category. Welding is another thermal treatment that generates residual stresses [5]. Residual stresses in stainless steel forgings induced by the forging process and water quenching are the concern of this article.

Effects of Residual Stresses

Regardless of their origin, the typical results of residual stress are difficulty machining due to shape change from residual stress relief and a reduced service life and difficulty machining. In Mickalonis and Dunn's experiments on stainless steel containers, the weld-induced residual stresses helped initiate stress corrosion cracking [5]. Withers and Bhadeshia [6] also explained that large mean values of tensile residual stresses on a part surface can severely shorten the fatigue life. There is a need for a simple, accurate way of predicting warm forging and quenching residual stresses so that they can be analyzed and reduced through process improvements.

Finite Element Simulation of Residual Stresses

Computer modeling has become a powerful method for predicting residual stresses that may be caused by any given metal processing method. However, any simulation result should be compared with experimental data. This comparison will reveal the accuracy of the material properties and conditions that are used in the simulation [7]. This is especially important when certain coefficients have a significant impact on numerical results. The heat transfer coefficient, for example, is a dynamic coefficient that changes with quench media chemistry, viscosity, and temperature. The heat transfer coefficient has a dramatic effect on the simulation results. The intent of the current research is to compare finite element results with experimental methods for residual stress measurement via neutron diffraction.

Measurement of Residual Stresses

Recently, much research has been devoted to developing, characterizing, and improving techniques for measuring residual stresses. In 2001, Withers and Bhadeshia listed methods such as hole drilling, curvature, X-ray diffraction, neutron diffraction, ultrasonic, magnetic, and Raman [6]. Only a few of these methods, however, are capable of accurate measurements for the large length scale of forgings. Robinson et al. found a general agreement between FEA predictions and neutron diffraction results for residual stresses in quenched 7449 aluminum blocks. FEA predicted a greater range of residual stress values and mostly over-predicted the residual stress when compared to neutron diffraction. The FEA predictions were typically within 1 standard deviation (35-41 MPa) of the measured residual stress (approx. -173 MPa) for the quenched sample [7]. The current study utilizes water quenched stainless steel forgings of a more complicated axisymmetric shape and compares FEA results with neutron diffraction measurements.

EXPERIMENTAL DETAILS

The 21-6-9 stainless steel pre-form is forged at approx. 950 °C into an axisymmetric cup shape (Figure 1). The forging process nearly doubles the yield strength from about 350 MPa to

about 650 MPa. The corresponding ultimate tensile strength increases from about 700 MPa to about 900 MPa.

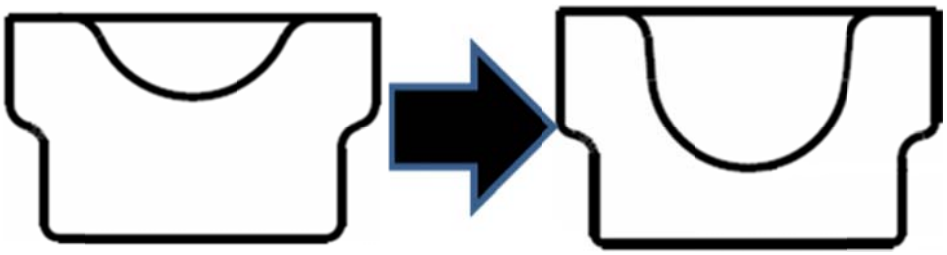

Figure 1. Schematic of the forging process.

Figure 2 shows a schematic of the HERF forging sample and the areas characterized in this work. Since austenitic stainless steel is subject to work hardening, the increase in yield strength and ultimate tensile strength within the forging is non-uniform. The final strength value in any given location within the forging depends on the amount of deformation strain applied to the microstructure in that location, and the temperature at which deformation is applied. It is important to note that the forging used for residual stress measurement had the top section mechanically removed after quenching. This likely resulted in some relieved residual stresses. Neutron scattering results were obtained in specific areas where result accuracy could be maximized and beam time minimized. These areas consisted of vertical lines at x positions -3.5, -6.2, -9, and -11.

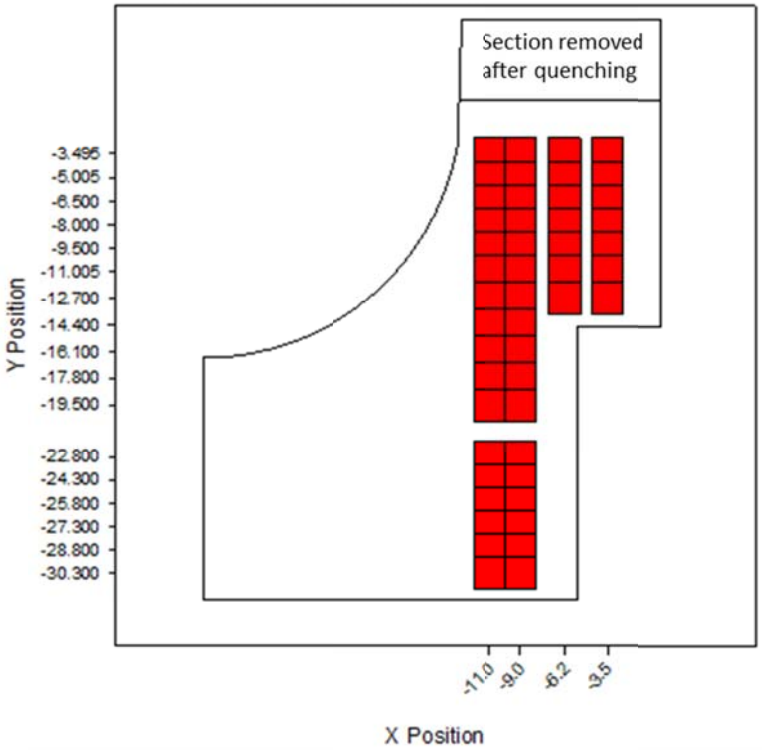

Figure 2. Schematic of the test areas for Neutron Scattering.

Neutron diffraction measurement of stress

The neutron diffraction measurements were completed on the SMARTS diffractometer at the Lujan Center at the Los Alamos Neutron Science Center (LANSCE), Los Alamos National Laboratory. Where possible, the experimental procedure followed the standard test method for determining residual stresses by neutron diffraction [8]. Details of SMARTS have been published elsewhere [9], and only a brief description will be given here.

SMARTS is a time-of-flight (TOF) diffractometer, with a continuous incident energy spectrum peaked at ~1.5 Å, but usable at wavelengths from 0.7 Å to 5.5 Å. The cross-section of the incident beam was defined by boron nitride apertures which were 3 mm wide and 12 mm high for the measurement of the radial and axial strains where the height of the slit has minimal influence on the along-wall resolution. The vertical slit was restricted to 3 mm close to the weld in the hoop and radial configuration where the height affects the along-wall resolution, and to 6 mm high well away from the weld where the strain gradients are small.

Two detector panels are located at ±90° from the incident beam and span ±15° in the vertical and horizontal planes. Because the incident neutron beam has a continuous energy spectrum, each detector panel records an entire diffraction pattern (d-spaces from 0.5 to 4 Å) simultaneously and with diffraction vectors bisecting the incident and diffracted beam vectors, i.e., at ±45° from the incident beam. Each detector is focused by a radial collimator to accept neutrons from a 3-mm section along the direction of the beam. The crossover of the incident beam and field of view of the radial collimators defines a “gauge” volume from which the diffraction data are collected and over which average lattice parameters are determined. The size of the gauge volume relative to the sample dimensions is roughly indicated in Figs. 1.

The sample was positioned optically with an accuracy of ±0.1 mm with the aid of two computerized Leicae theodolites. The sample position was verified by “wall scans” of the surface through the gauge volume. The sample was mounted on a sturdy fixture, which could be rotated about a horizontal axis (manually) to bring the cylinder axis of the sample either vertical or horizontal. When the sample axis was horizontal, the two banks recorded the axial (+90° bank) and radial (-90° bank) strains and, when it was vertical, the two banks recorded the radial (+90° bank) and hoop (-90° bank) strains. The measurements of the radial strains were repeated in the two configurations (in different detector banks) and agreed to within uncertainty.

The sample was swept through the gauge volume by a motorized translator table, and the lattice parameters were mapped as a function of position. The neutron diffraction collection times were 20–30 min per point, depending on the gauge volume used. Each diffraction pattern was analyzed by Rietveld refinement using the General Structural Analysis Software (GSAS) [10] developed at LANSCE. Pertinent to this study, the three lattice parameters, a, b and c, were determined by the refinement as well as the pole density of many hkls in the diffraction pattern along the specific sample directions.

The residual strains are calculated from the fractional difference of the spatially varying lattice parameters relative to appropriate reference lattice parameters, a_{ref}, b_{ref} and c_{ref}, for example

$$\varepsilon_\alpha = (\alpha - \alpha_{ref})/\alpha_{ref} \quad (1)$$

Reference coupons were machined from another forging and reference lattice parameter measurements were completed at the time of the residual stress measurement in the forged sample according to the preferred procedure [8,11]. To determine a representative macroscopic strain field from the observed lattice strains, the three lattice strains were averaged with weighting based on their measured textural strength along each sample direction, e.g.,

$$\varepsilon_{macro} = \sum_{i=a,b,c} \omega_i \, \varepsilon_i \quad (2)$$

This method accounts for the texture evolution from the base metal to the weld and corresponds to that outlined by Daymond [12] for determining representative residual strains from anisotropic crystals, except the lattice parameters (a, b, and c) obtained from Rietveld refinement were used instead of multiple single peaks (hkl) because of practical intensity considerations.

ModelingProcedures

As the part is not annealed after forming, the forging and quench processes should be modeled sequentially. However, technical challenges have so far prevented the models from running successfully. Separate simulations of each step were run. The forging step was performed with Abaqus/Explicit [13] with C3D8R elements - 8-node linear bricks, reduced integration, with hourglass control. The die and punch were modeled as fully rigid bodies. A stress-strain curve was developed at the forging temperature of 950°C via Sandia material testing [13]. Simulation of the quenching process was performed in Abaqus/Standard [14]. As the final deformations are negligible, it was assumed the heat transfer model was not dependent on the solid mechanics model, and a sequentially coupled analysis could be used. In this type of analysis, nodal temperatures obtained during a heat transfer analysis are transferred to a solid mechanics analysis to induce thermal stresses; but the resulting geometry changes are not looped back to the thermal model. The heat transfer portion of quenching was modeled with DC3D8 elements 8 node linear heat transfer bricks. After transfer to the solid mechanics step, C3D8 elements 8 node linear bricks were used. The part was assumed to be at an initial uniform temperature of 950°C. Heat loss from quenching was modeled as a surface interaction with a surface temperature dependent film coefficient. When the heat transfer analysis completed, the nodal temperatures were transferred to the solid mechanics analysis to drive thermal stresses. Temperature dependent stress-strain curves were adapted from Chiesa, M.L et. al [15]. For all analyses, the forging was modeled using quarter symmetry with appropriate symmetry boundary conditions. Residual strains were extracted from the thermal stress and forging analyses at locations matching those in physical testing. The Abaqus variable Elastic Strain (EE) was used for the thermal stress analysis. EE is not available in explicit analyses, so it could not be directly recovered from the forging analysis, and was therefore calculated from residual stresses and the expanded Hooke's law [16]:

$$\varepsilon_x = \frac{1}{E}[\sigma_x - \nu(\sigma_y + \sigma_z)] \quad (3)$$

In the model's global coordinate system, on the X symmetry plane ε_x = Hoop strain, ε_y = Axial Strain, and ε_z = Radial strain.

Results and Discussion

The results from neutron diffraction and modeling can be shown in many different ways. In this paper they have been broken into their directional components, axial, radial, and hoop residual strains. The comparison of results from simulation to the neutron scattering data will be limited to these areas (Figure 2). Due to the size and shape of the part very limited amounts of hoop residual strain data was able to be captured. This makes accurate correlation between the model and the neutron scattering results difficult. The neutron scattering results for residual strain are shown on contour plots in Figure 3. Qualitatively, the highest residual strain is seen in the hoop direction and is compressive. There are also some high tensile residual strains in the axial and radial directions near the top of the forging.

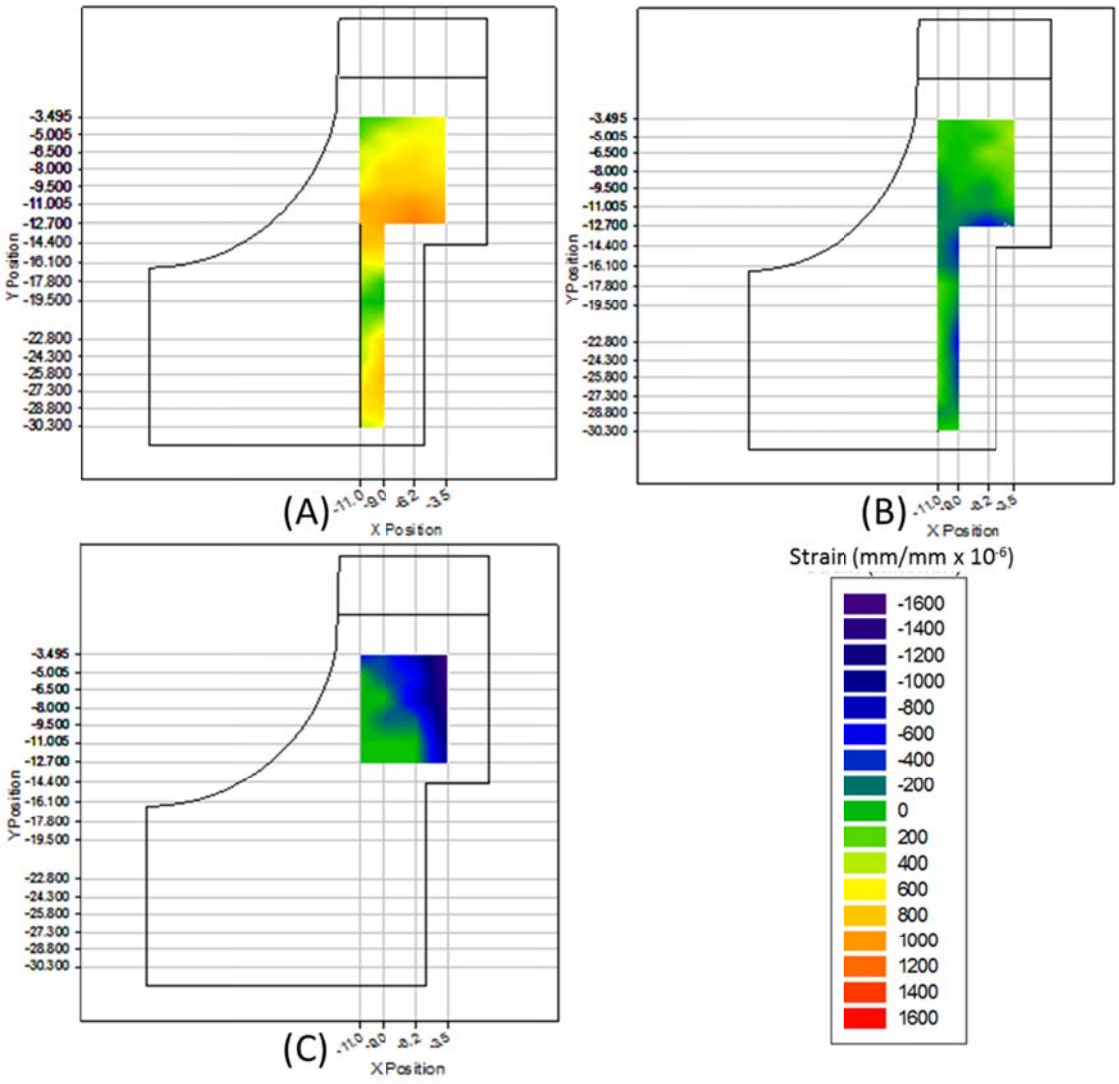

Figure 3. Contour plots of the radial (A), axial (B), and hoop (C) residual strains measured using neutron scattering.

In Figure 4 the difference between various quenching rates in simulation are shown. When the highest quenching rate is used, the results are much higher in magnitude and are more sensitive to the shape of the forging. With the intermediate quench rate values the trend is more realistic and shows little variation with large h value changes. For comparison to the measured results, quenching simulation results for the h value of 7000 were used.

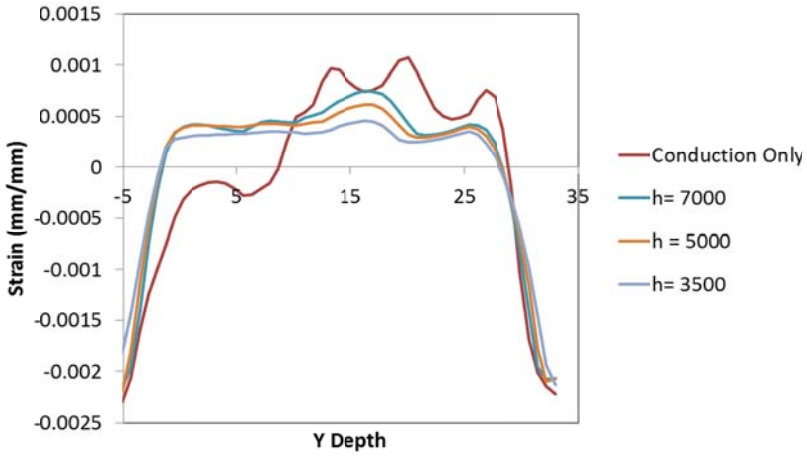

Figure 4. Hoop residual strain quench simulation results for data at the -11 x position.

The simulation results for forging a residual strain free part show compressive residual strain in the hoop direction near the top of the forging, and slightly tensile residual strains in the axial direction as well as slightly compressive residual strains in the radial direction near the bottom (Figure 5A). The simulation results for quenching from a strain free state show tension in the hoop and axial directions near the top of the forging, with compressive residual strain in the radial direction in the same region (Figure 5B).

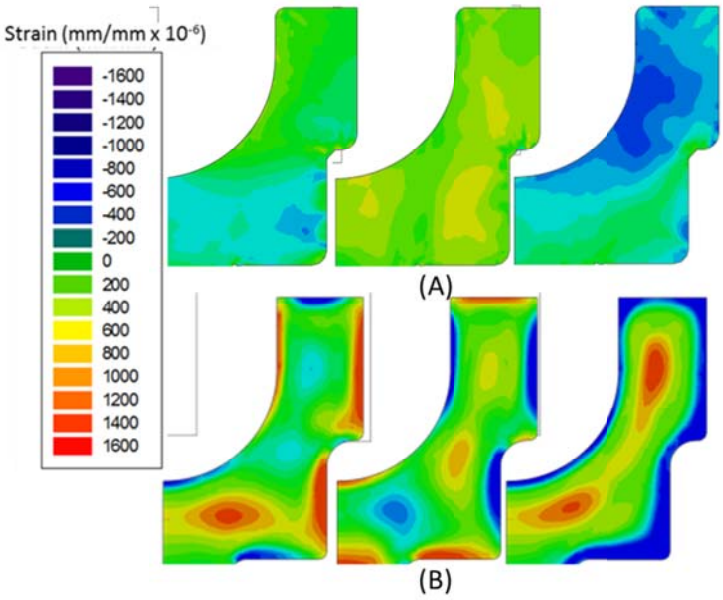

Figure 5. From left to right radial, axial and hoop strains for forging simulation (A), and quenching simulation (B).

The residual strain results from simulation for the forging process step and the quenching process step are not additive. Simple addition of the residual strain values does not provide good correlation to the measured results as shown in Figure 6.

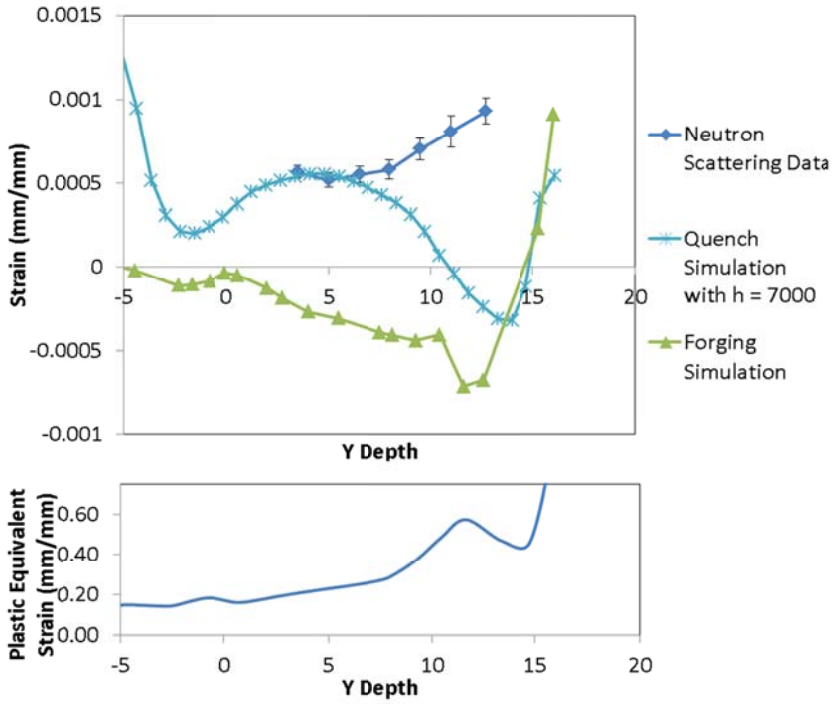

Figure 6. A comparison of simulation results to experimental results for data collected at x position -3.5.

This means there is some interaction between the two process steps. When the various residual strain results are compared to the plastic strain results from the forging process some correlation is evident. For austenitic stainless steel it has been shown that plastic strain values up to approximately 0.7 PEEQ (plastic equivalent strain) during warm forging can strain harden the material without causing recrystallization [2]. As shown in the bottom graph of Figures 6 and 7, when the PEEQ values for the forging step are considered, the deviation of the neutron scattering values from the strains correlate with areas of higher strains. When the PEEQ strain is high enough to strengthen the material the corresponding residual strain measured with neutron scattering deviates from the simulation data. Figure 7 shows a peak in PEEQ that matches well with the area of measured data above the simulated residual strain. This suggests that the higher yield strength reduces the deformation caused by the quench step, but increases the residual strain.

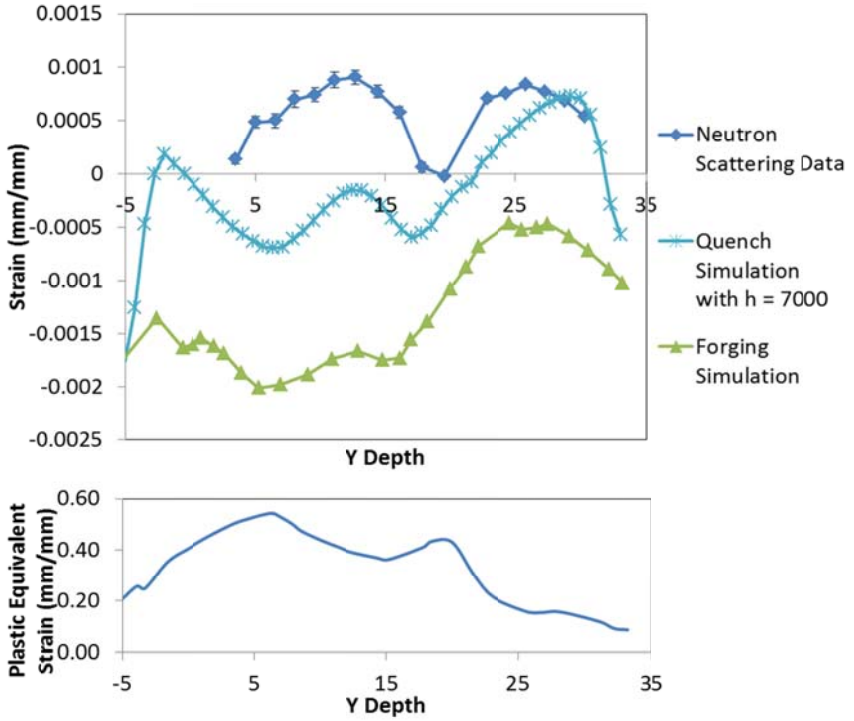

Figure 7. A comparison of simulation results to experimental results for data collected at x position -9.

In figure 8, the comparison of strain values shows that at 0 degrees and 60 degrees the strain trends and magnitudes are similar. The differences in the results are likely due to one or more of several factors. The forgings could have been forged slightly off center causing higher deformation on one side. The quench could have been non-uniform due to the method of transfer, directional water flow, or the forgings orientation during quenching.

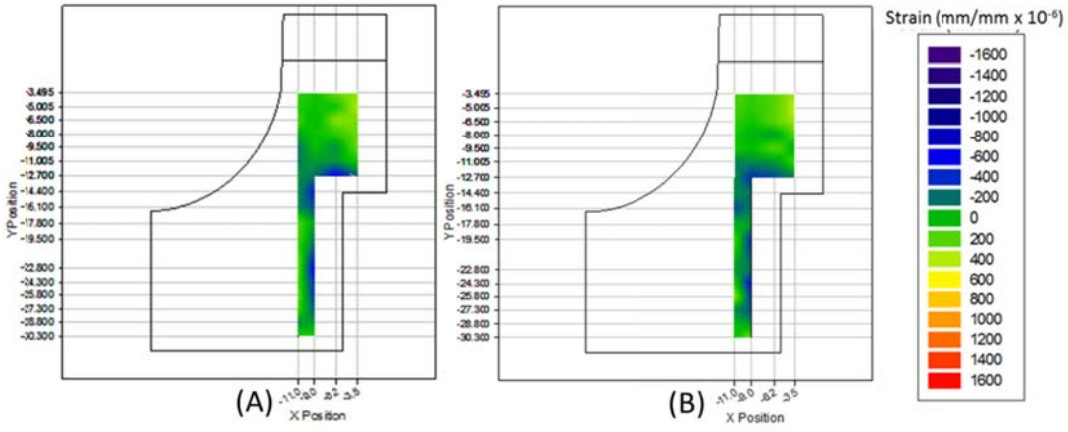

Figure 8. Radial strain contour plots for data taken at 0 degrees (A) and 60 degrees (B).

CONCLUSION

Warm forging, water quenching, and machining processes have a severe effect on residual stresses when taken as a whole. Computer simulation of these residual stresses is challenging, even when taken as piece-wise processes. An extremely accurate knowledge of heat transfer, degree of deformation, cooling rate, thermal boundary effects, and other parameters is essential for accurate prediction of resulting residual stresses. The model is not yet mature enough for independent prediction. However, it is now understood that areas of a 21-6-9 forging (work hardening material) with higher strain hardening, and therefore higher strength, can produce higher residual stresses because they have a higher elastic deformation range. In regions of higher strain hardening there tends to be higher deviation from the FEA predicted residual stress since forging deformation and residual stresses were not considered during quenching simulation. Additional work is needed on coupling of the forging and quenching processes in the simulation. The heat transfer during quenching also needs higher fidelity determination. Material removal processes must be taken into account and simulated as well, as this process tends to shift residual stresses in the part.

REFERENCES

[1] McQueen, H.J. The production and utility of recovered dislocation substructures. Metallurgical Transactions A 8A, 1977, pp 807–823.
[2] Switzner, N.T., Van Tyne, C.J., and Mataya, M.C., Effect of forging strain rate and deformation temperature on the mechanical properties of warm-worked 304L stainless steel. Journal of Materials Processing Technology, vol. 210, 2010. pp. 8, 998-1007.
[3] Prime, M.P., Newborn, M.A., Balog, J.A. Quenching and Cold-Work Residual Stresses in Aluminum and Hand Forgings: Contour Method Measurement and FEM Prediction. Materials Science Forum Vols 426-432 (2003) (proc. Of THERMEC'2003: Processing and Manufacturing of Advanced Materials, July 7-11, Leganes, Madrid, Spain.)
[4] Withers, P.J. and Bhadeshia, H.K.D.H. Residual Stress: Part 2 – Nature and Origins. Materials Science and Technology. April 2001, Vol 17, pp 366-375.
[5] Mickalonis, J.I. and Dunn, K.A. Residual Stresses in 3013 Containers. Laboratory Report: SRNL-STI-2009-00732, 2009.
[6] Robinson, J.S., Tanner, D.A., Truman, C.E., Wimpory, R.C., 2010. Measurement and prediction of machining induced redistribution of residual stress in the aluminium alloy 7449. Society for Experimental Mechanics. Published online: 12 August 2010. DOI 10.1007/s11340-010-9389-4.)
[7] Withers, P.J. and Bhadeshia, H.K.D.H. Residual Stress: Part 1 – Measurement Techniques. Materials Science and Technology. April 2001, Vol 17, pp 355-365.
[8] Vamas-20. Technical specification, ISO/TS 21432; 2005.
[9] Bourke M, Dunand D, Ustundag E. Appl Phys A 2002;A74:S1707.
[10] Vondreele RB, Jorgensen JD, Windsor CG. J Appl Cryst 1982;15:581.
[11] Hutchings MT, Withers PJ, Holden TM, Lorentzen T. Introduction to the characterization of residual stress by neutron diffraction. Boca Raton, FL: Taylor & Francis; 2005.

[12] Daymond MR. J Appl Phys 2004;96:4263.
[13] Kassner, M.E., and Breithaupt, R.D. The Yield Stress of Type 21-6-9 Stainless Steel Over a Wide Range of Strain Rate and Temperature. Proceedings of the Institute of Physics' 3rd Conference on Mechanical Properties at High Rates of Strain, Oxford, England, 1984, pp 47-54.
[14] ABAQUS Version 6.9. Manual, Dassault Systèmes, 2009.
[17] Chiesa, M.L., Antoun, B.R., Brown, A.A., Regueiro, R.A., Ostien, J., Jones, R., Bammann, D.J., Yang, N., Using Modeling and Simulation to Optimize Forged Material Properties. Proceedings of the 25th Forging Industry Technical Conference, April 19-21, 2004, Detroit, MI, Cleveland, OH. (cannot find page numbers).
[18] Young, W.C., Budynas, R.G., Roark's Formulas for Stress and Strain, Seventh Edition, Copyright 2002, McGraw-Hill Companies, Inc., New York. pp 15.